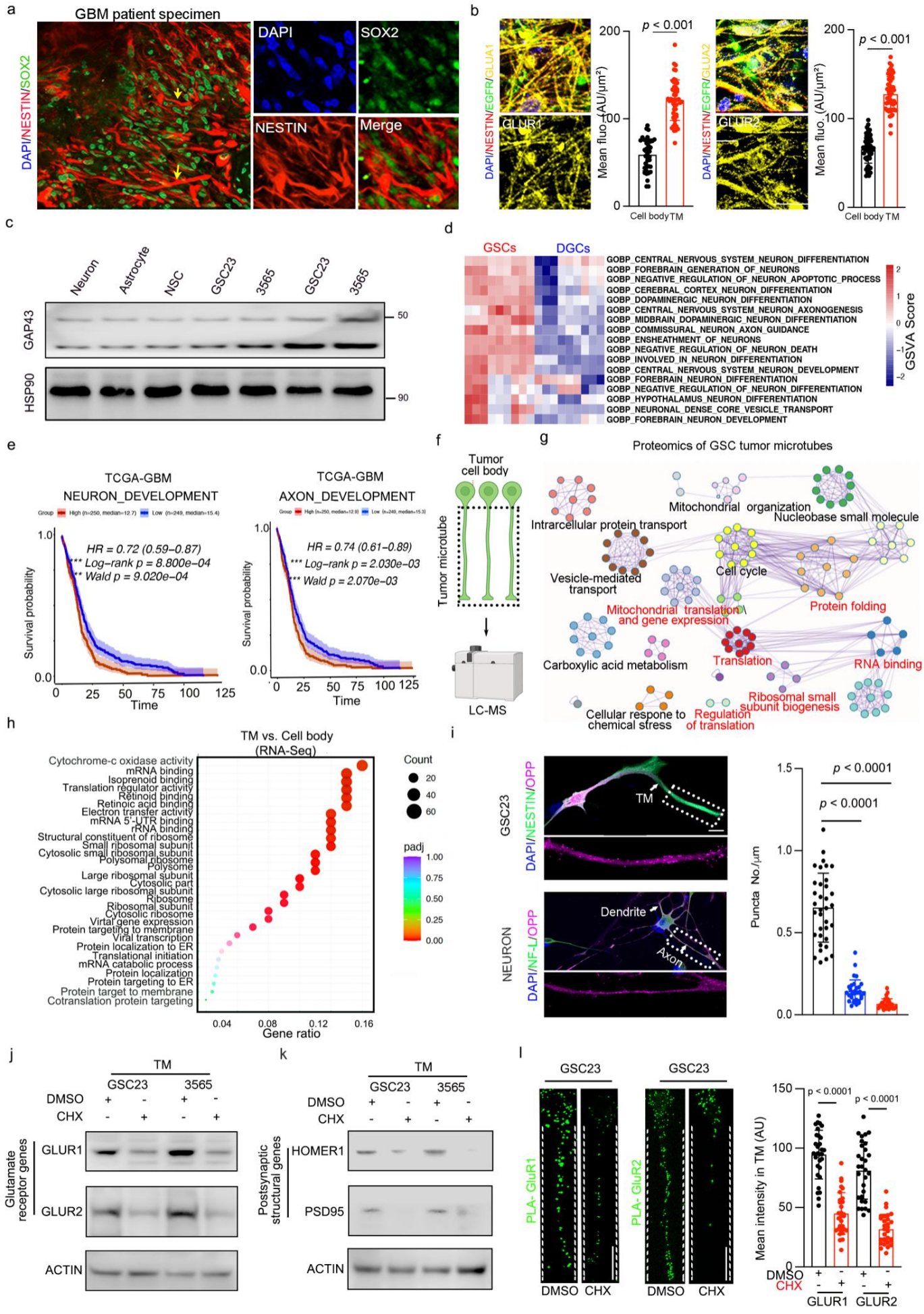
a
GBM patient specimen
DAPI/NESTIN/SOX2
DAPI
SOX2
NESTIN
Merge
b
DAPI/NESTIN/EGFR/GLUA1
GLUR1
p < 0.001
Mean fluo. (AU/μm²)
Cell body
TM
DAPI/NESTIN/EGFR/GLUA2
GLUR2
p < 0.001
c
Neuron
Astrocyte
NSC
GSC23
3565
GSC23
3565
GAP43
HSP90
50
90
d
GSCs
DGCs
GOBP_CENTRAL_NERVOUS_SYSTEM_NEURON_DIFFERENTIATION
GOBP_FOREBRAIN_GENERATION_OF_NEURONS
GOBP_NEGATIVE_REGULATION_OF_NEURON_APOPTOTIC_PROCESS
GOBP_CEREBRAL_CORTEX_NEURON_DIFFERENTIATION
GOBP_DOPAMINERGIC_NEURON_DIFFERENTIATION
GOBP_CENTRAL_NERVOUS_SYSTEM_NEURON_AXONOGENESIS
GOBP_MIDBRAIN_DOPAMINERGIC_NEURON_DIFFERENTIATION
GOBP_COMMISSURAL_NEURON_AXON_GUIDANCE
GOBP_ENSHEATHMENT_OF_NEURONS
GOBP_NEGATIVE_REGULATION_OF_NEURON_DEATH
GOBP_INVOLVED_IN_NEURON_DIFFERENTIATION
GOBP_CENTRAL_NERVOUS_SYSTEM_NEURON_DEVELOPMENT
GOBP_FOREBRAIN_NEURON_DIFFERENTIATION
GOBP_NEGATIVE_REGULATION_OF_NEURON_DIFFERENTIATION
GOBP_HYPOTHALAMUS_NEURON_DIFFERENTIATION
GOBP_NEURONAL_DENSE_CORE_VESICLE_TRANSPORT
GOBP_FOREBRAIN_NEURON_DEVELOPMENT
GSVA Score
e
TCGA-GBM
NEURON_DEVELOPMENT
HR = 0.72 (0.59–0.87)
*** Log–rank p = 8.800e–04
** Wald p = 9.020e–04
Survival probability
Time
TCGA-GBM
AXON_DEVELOPMENT
HR = 0.74 (0.61–0.89)
*** Log–rank p = 2.030e–03
** Wald p = 2.070e–03
f
Tumor cell body
Tumor microtube
LC-MS
g
Proteomics of GSC tumor microtubes
Intracellular protein transport
Mitochondrial organization
Nucleobase small molecule
Vesicle-mediated transport
Cell cycle
Mitochondrial translation and gene expression
Protein folding
Carboxylic acid metabolism
Translation
RNA binding
Ribosomal small subunit biogenesis
Cellular respone to chemical stress
Regulation of translation
h
TM vs. Cell body (RNA-Seq)
Cytochrome-c oxidase activity
mRNA binding
Isoprenoid binding
Translation regulator activity
Retinoid binding
Retinoic acid binding
Electron transfer activity
mRNA 5'-UTR binding
rRNA binding
Structural constituent of ribosome
Small ribosomal subunit
Cytosolic small ribosomal subunit
Polysomal ribosome
Polysome
Large ribosomal subunit
Cytosolic part
Cytosolic large ribosomal subunit
Ribosome
Ribosomal subunit
Cytosolic ribosome
Virtal gene expression
Protein targeting to membrane
Viral transcription
Protein localization to ER
Translational initiation
mRNA catabolic process
Protein localization
Protein targeting to ER
Protein target to membrane
Cotranslation protein targeting
Gene ratio
Count
padj
i
GSC23
DAPI/NESTIN/OPP
TM
NEURON
DAPI/NF-L/OPP
Dendrite
Axon
p < 0.0001
p < 0.0001
Puncta No./μm
j
TM
GSC23
3565
DMSO
CHX
Glutamate receptor genes
GLUR1
GLUR2
ACTIN
k
TM
GSC23
3565
DMSO
CHX
Postsynaptic structural genes
HOMER1
PSD95
ACTIN
l
GSC23
GSC23
PLA- GluR1
PLA- GluR2
DMSO
CHX
DMSO
CHX
p < 0.0001
p < 0.0001
Mean intensity in TM (AU)
DMSO
CHX
GLUR1
GLUR2

Extended Data Figure 1. Neuron–glioma synapse formation is dependent on local protein synthesis.

a, Representative immunofluorescence staining of DAPI (blue), NESTIN (red), and SOX2 (green) in GSC23. Scale bars: 100 μm.

b, Patient-derived glioblastoma surgical biopsy specimens underwent immunofluorescent staining for a tumor cell marker [EGFR (green)], stem cell marker [Nestin (magenta)], neurotransmitter receptor [GluR1, GluR2 (yellow)], and general marker of nuclei [DAPI (blue)]. Representative images are shown. Scale bar: 40 μm. Right: Quantitative analysis of immunofluorescence intensity in cell body and TM.

c, Western blot analysis of the expression of GAP43 in different cell types (GSCs, DGCs, NSC ENSA, neuron, and astrocyte).

d, The GSVA analysis results of neuronal development-related gene sets in GSCs and DGCs. Rows represent different GOBP terms. The heatmap colors range from blue to red, corresponding to GSVA scores from low to high.

e, Kaplan–Meier overall survival analysis based on neuronal development and axon development gene signatures in IDH-wildtype glioma patients from the TCGA cohort.

f, Schematic depicting experimental setup. Glioma cells were cultured in one compartment of a microfluidic device; After 7 days, compartments were separately lysed for proteomic analysis.

g, Functional analysis of the proteome identified within TMs. A network diagram was constructed with enriched terms as nodes and similarities as edges. Each color of the nodes represented a various term.

h, Transcriptome analysis of separated TMs and cell bodies.

i, Representative fluorescence images for puromycin incorporation in GSC23. OPP incorporation was detected by labeling with Alexa Fluor 647 using Click chemistry. DAPI (blue), Nestin (green) or NF-L (green), OPP (Magenta). Right: Quantitative analysis of immunofluorescence intensity in GSC23 TM, neuon (axon and dendrite). Scale bar: 10 μm.

j, Patient-derived GSCs were treated with either vehicle control (DMSO) or CHX for 12 hours. TMs were harvested, resolved by SDS-PAGE, and immunoblotted for AMPA receptors (GluR1 and GluA2). ACTIN was used as a loading control.

k, Patient-derived GSCs were treated with either vehicle control (DMSO) or CHX for 12 hours. TMs were harvested, resolved by SDS-PAGE, and immunoblotted for markers of postsynaptic structures (HOMER1 and PSD95). ACTIN was used as a loading control.

l, Left: Patient-derived GSCs (GSC23) were cultured with either vehicle control (DMSO) or cycloheximide (CHX (10 μg/ml)) for 12 hours to inhibit protein translation. Proximity ligation assays (PLAs) were used to detect nascent GLUR1 (left) or GLUR2 (right) in TMs. Scale bar: 40 μm. Right: Data were quantified from cells from more than 3 chambers per condition in three independent experiments. DMSO, n = 64; CHX, n = 50.

Representative of three independent experiments in a, b, i-l. Data are presented as mean ± SD. One-way ANOVA followed by multiple comparisons with adjusted p-values for i and l. log-rank test for e.

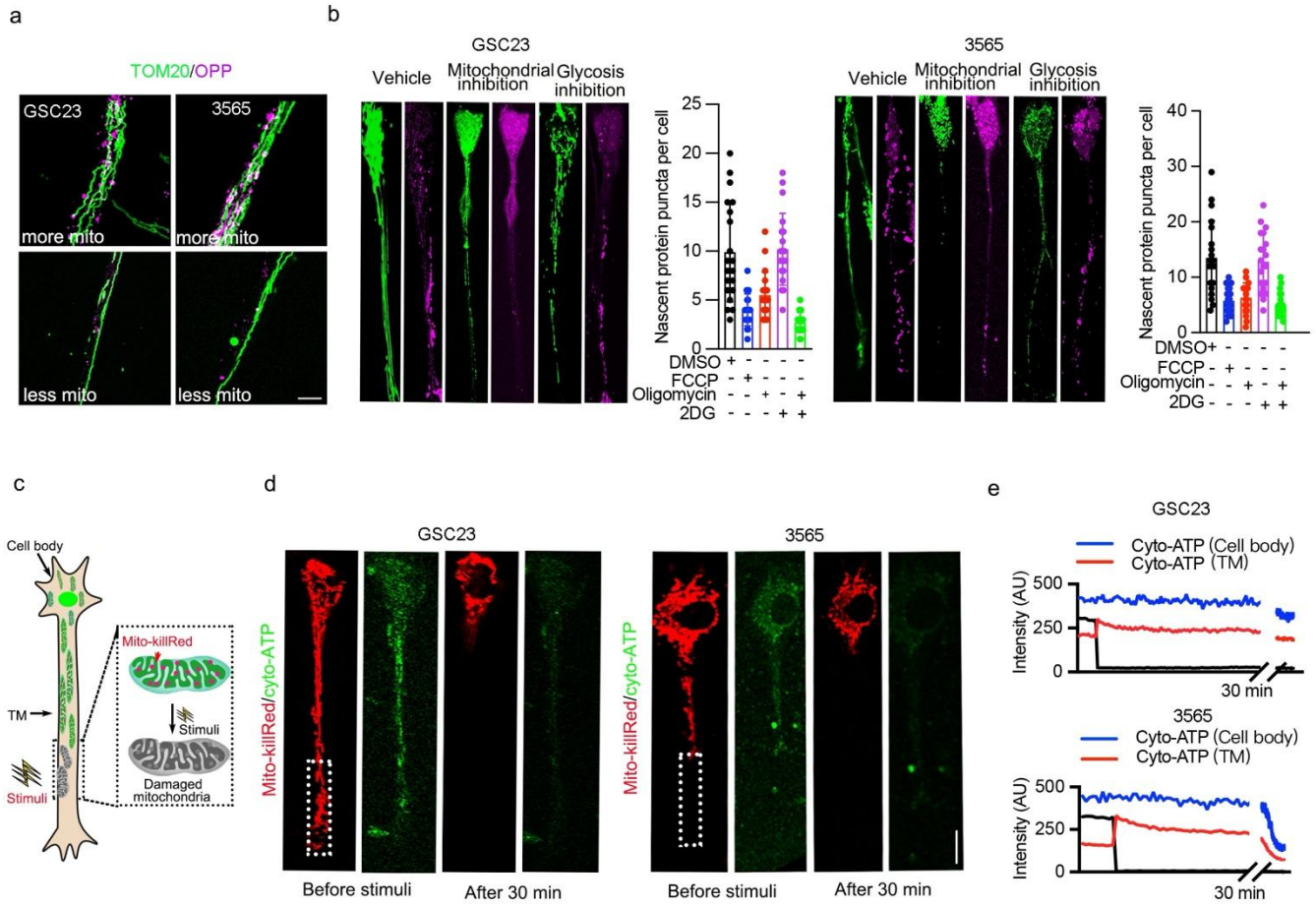
a
TOM20/OPP
GSC23
3565
more mito
more mito
less mito
less mito
b
GSC23
Vehicle
Mitochondrial inhibition
Glycosis inhibition
Nascent protein puncta per cell
DMSO
FCCP
Oligomycin
2DG
3565
Vehicle
Mitochondrial inhibition
Glycosis inhibition
Nascent protein puncta per cell
DMSO
FCCP
Oligomycin
2DG
c
Cell body
TM
Stimuli
Mito-killRed
Stimuli
Damaged mitochondria
d
GSC23
3565
Mito-killRed/cyto-ATP
Mito-killRed/cyto-ATP
Before stimuli
After 30 min
Before stimuli
After 30 min
e
GSC23
Cyto-ATP (Cell body)
Cyto-ATP (TM)
Intensity (AU)
30 min
3565
Cyto-ATP (Cell body)
Cyto-ATP (TM)
Intensity (AU)
30 min
f
GSC23
Before stim
After 30 min
Relative ATP intensity (%)
TM
cell body
3565
Before stim
After 30 min
Relative ATP intensity (%)
TM
Cell body
g
GFP/Mito-killred
GSC23
3565
Stimulation at TM
Stimulattion at cell body
GSC23
TM stimulation
Cell body stimulation
Retraction speed (μm/min)
3565
TM stimulation
Cell body stimulation
Retraction speed (μm/min)
h
GSC23
3565
DAPI/FASTKD2
Cell body
TM
TM
Cell body
Puncta No. /μm

Extended Data Figure 2. Mitochondrial protein FASTKD2 maintains local protein synthesis and TM formation.

a, Representative fluorescent images of nascent protein puncta (OPP, magenta) and mitochondria (TOM20, green) in GSCs. Nascent protein puncta were detected by labeling with Alexa Fluor 647 using Click chemistry. Scale bar: 40 μm.

b, Left: Representative fluorescent images of nascent protein puncta (OPP, magenta) and mitochondria (TOM20, green) in GSCs in the presence of FCCP (mitochondrial inhibition) and 2DG (glycolysis inhibition) treatment. Right: Quantitative analysis of nascent protein puncta in the presence of various drug treatment combinations for 12 hours. The following drugs were used: FCCP (1 μM), oligomycin (100 ng/ml), 2DG (3 mM). (n = 20 cells). Scale bar: 40 μm.

c, Schematic depicting experimental setup. Mito-killRed was utilized to locally damage mitochondria and evaluate the influence on protein synthesis in TMs.

d, Immunofluorescent imaging after GSCs were co-transfected with a cytoplasmic ATP reporter (cyto-ATP) and Mito-killRed. The white box denotes the site of laser stimulation, and the yellow circle indicates the location used for ATP detection.

e, The intensity of cyto-ATP was measured via a time course to assess ATP levels in response to laser stimulation.

f, Quantitative analysis of ATP concentration after laser stimulation for 30 minutes in GSCs. (n = 3).

g, GSCs were transfected with GFP and Mito-killRed. The change in the length of the TM, represented by retraction speed, was measured and quantified. (n = 3). **, $p < 0.01$. Scale bar: 20 μm.

h, Representative fluorescent images of FASTKD2 (green) and DAPI (blue) nuclei in GSCs. And Quantitative analysis of immunofluorescence intensity in the GSCs TM and cell body, Scale bar: 20 μm.

Representative of three independent experiments in a-h. Data are presented from three independent experiments in b and f-h. data are presented as mean ± SD. Student's t-test with p-values for g. One-way ANOVA followed by multiple comparisons with adjusted p-values for b, f, and h.

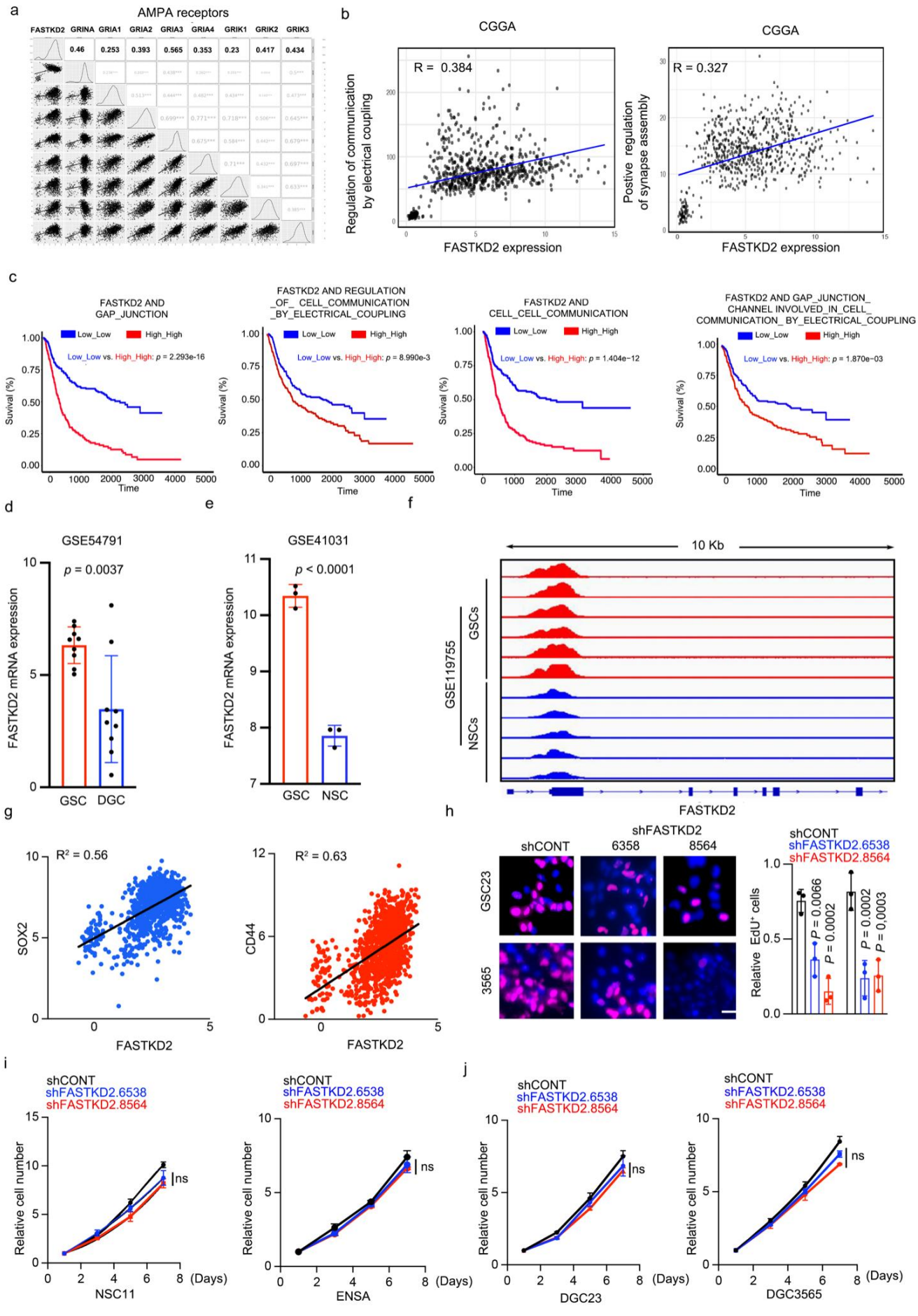
a
AMPA receptors
FASTKD2 GRINA GRIA1 GRIA2 GRIA3 GRIA4 GRIK1 GRIK2 GRIK3
0.46 0.253 0.393 0.565 0.353 0.23 0.417 0.434
b
CGGA
R = 0.384
Regulation of communication by electrical coupling
FASTKD2 expression
CGGA
R = 0.327
Postive regulation of synapse assembly
FASTKD2 expression
c
FASTKD2 AND GAP_JUNCTION
Low_Low High_High
Low_Low vs. High_High: p = 2.293e-16
Suvival (%)
Time
FASTKD2 AND REGULATION _OF_ CELL_COMMUNICATION _BY_ELECTRICAL_COUPLING
Low_Low High_High
Low_Low vs. High_High: p = 8.990e-3
Suvival (%)
Time
FASTKD2 AND CELL_CELL_COMMUNICATION
Low_Low High_High
Low_Low vs. High_High: p = 1.404e-12
Suvival (%)
Time
FASTKD2 AND GAP_JUNCTION_ CHANNEL INVOLVED_IN_CELL_ COMMUNICATION_ BY_ELECTRICAL_COUPLING
Low_Low High_High
Low_Low vs. High_High: p = 1.870e-03
Suvival (%)
Time
d
GSE54791
p = 0.0037
FASTKD2 mRNA expression
GSC DGC
e
GSE41031
p < 0.0001
FASTKD2 mRNA expression
GSC NSC
f
10 Kb
GSE119755
GSCs
NSCs
FASTKD2
g
R² = 0.56
SOX2
FASTKD2
R² = 0.63
CD44
FASTKD2
h
shCONT
shFASTKD2
6358
8564
GSC23
3565
shCONT
shFASTKD2.6538
shFASTKD2.8564
Relative EdU⁺ cells
P = 0.0066
P = 0.0002
P = 0.0002
P = 0,0003
i
shCONT
shFASTKD2.6538
shFASTKD2.8564
Relative cell number
ns
(Days)
NSC11
shCONT
shFASTKD2.6538
shFASTKD2.8564
Relative cell number
ns
(Days)
ENSA
j
shCONT
shFASTKD2.6538
shFASTKD2.8564
Relative cell number
ns
(Days)
DGC23
shCONT
shFASTKD2.6538
shFASTKD2.8564
Relative cell number
ns
(Days)
DGC3565

Extended Data Figure 3. FATSKD2 portends poor prognosis in GBM and maintains stemness.

a, The correlation between FASTKD2 expression and AMPA receptors in CGGA database.

b, The correlation between FASTKD2 expression and regulation of communication related pathways.

c, Combined Kaplan–Meier survival analysis of FASTKD2 expression and the regulation of communication related pathways in the CGGA.

d, FASTKD2 expression levels in GSCs and matched DGCs using publicly available dataset GSE41031. (GSC, n = 8, DGC, n = 9).

e, FASTKD2 expression levels in GSCs and NSCs using publicly available dataset GSE54791. (n = 3).

f, H3K27ac ChIP-seq enrichment tracks at FATSKD2 gene loci in GSCs and NSCs using publicly available dataset GSE119755.

g, Pairwise correlation analysis between FASTKD2 and stemness markers (SOX2, CD44) was investigated using the CGGA database. R2 values indicate the correlation.

h, Representative immunofluorescence images of EdU incorporation assays in GSC23 and 3565 cells transduced with control shRNA (shCONT) or FASTKD2-targeting shRNAs (6358 and 8564). EdU (magenta) indicates proliferating cells, and DAPI (blue) indicates nuclei. Scale bar, 40 μm

i, Cell viability was measured in NSCs transduced with either shCONT or shFASTKD2. (n = 3).

j, Cell viability was measured in DGCs transduced with either shCONT or shFASTKD2. (n = 3).

Representative of three independent experiments in h. Data are presented from three independent experiments in i-j. data are presented as mean ± SD. Two-tailed Student's t-test with p values for d, and e. Two-way ANOVA followed by multiple comparisons with adjusted p-value. ns, not significant. log-rank test for c.

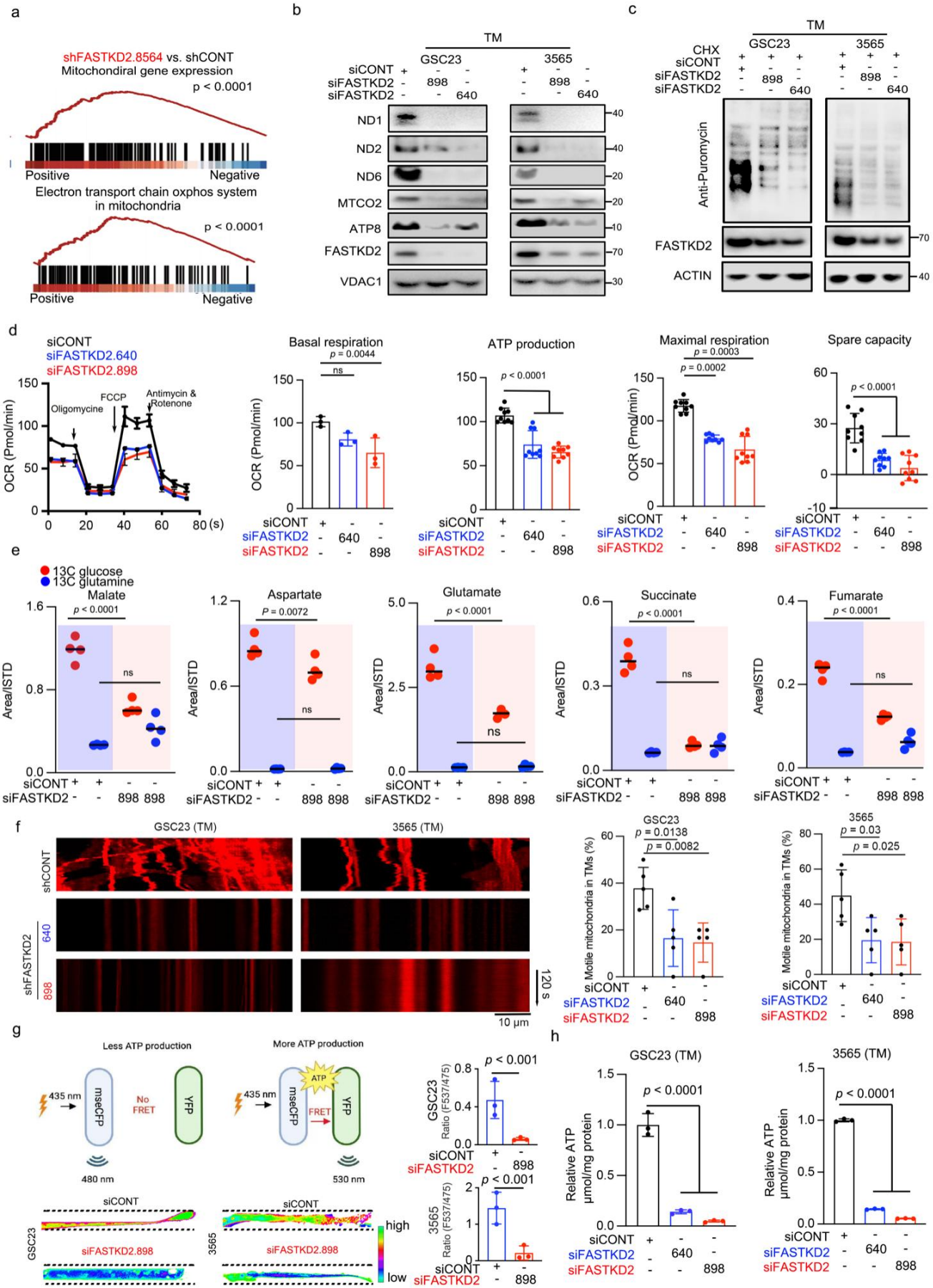
a
shFASTKD2.8564 vs. shCONT
Mitochondiral gene expression
p < 0.0001
Positive
Negative
Electron transport chain oxphos system in mitochondria
p < 0.0001
Positive
Negative
b
TM
GSC23
3565
siCONT
siFASTKD2
siFASTKD2
898
640
ND1
ND2
ND6
MTCO2
ATP8
FASTKD2
VDAC1
c
TM
GSC23
3565
CHX
siCONT
siFASTKD2
siFASTKD2
898
640
Anti-Puromycin
FASTKD2
ACTIN
d
siCONT
siFASTKD2.640
siFASTKD2.898
OCR (Pmol/min)
Oligomycine
FCCP
Antimycin & Rotenone
(s)
Basal respiration
p = 0.0044
ns
ATP production
p < 0.0001
Maximal respiration
p = 0.0003
p = 0.0002
Spare capacity
p < 0.0001
e
13C glucose
13C glutamine
Malate
p < 0.0001
Aspartate
P = 0.0072
Glutamate
p < 0.0001
Succinate
p < 0.0001
Fumarate
p < 0.0001
Area/ISTD
ns
siCONT
siFASTKD2
898
640
f
GSC23 (TM)
3565 (TM)
shCONT
shFASTKD2
640
898
120 s
10 μm
GSC23
p = 0.0138
p = 0.0082
3565
p = 0.03
p = 0.025
Motile mitochondria in TMs (%)
g
Less ATP production
More ATP production
435 nm
mseCFP
YFP
No FRET
FRET
ATP
480 nm
530 nm
siCONT
siFASTKD2.898
GSC23
3565
high
low
p < 0.001
GSC23 Ratio (F537/475)
3565 Ratio (F537/475)
h
GSC23 (TM)
3565 (TM)
p < 0.0001
Relative ATP μmol/mg protein

Extended Data Figure 4. FASTKD2 maintains mitochondrial function and ATP production in GSC TMs.

a, Analysis of FASTKD2 immunoprecipitated by polyacrylamide gel electrophoresis and silver staining.

b, Western blot analysis evaluating mitochondrial-related protein expression in GSCs after FASTKD2 knockdown.

c, Mitochondrial protein synthesis in GSCs were assessed in the presence or absence of FASTKD2 knockdown. Cells were treated with 50μg/ml cycloheximide (CHX) for 20minutes prior to puromycin treatment for 15minutes. Purified mitochondrial lysates were probed with anti-puromycin antibody to measure mitochondrial protein synthesis.

d, Real-time measurements and line graph representation of the oxygen consumption rate (OCR) in GSCs as measured by Seahorse XF96. After basal OCR was obtained, oligomycin (1 μM) was added to determine proton leak-linked OCR and calculate ATP-linked OCR. The uncoupler FCCP (1 μM) was then added, and the maximal OCR was measured. Finally, excess OCR was obtained after adding antimycin A (1 μM) and rotenone (1 μM) to inhibit the electron transport chain. (n = 3).

e, The metabolite profiling in GSC23 TMs, GSC23 cells treated with siCONT and siFASTKD2.898 for 48 hours, cells were labeled with [U-^{13}C] glucose and [U-^{13}C] glutamine to trace metabolic fluxes. Red and blue dots represent individual values calculated using [U-13C] glucose and [U-13C] glutamine, respectively, (n = 4).

f, Kymograph showing the motility of mitochondria labeled with DsRed-mito in GSC TMs. Scale bars in all panels, 10 μm. Qualification of motility of the mitochondria labeled with DsRed-mito in GSC TMs (n = 5).

g, Left: Schematic drawing of FRET-based ATP probes. Middle: Cytoplasmic ATP concentration was measured using the ATP sensor ATeam transfected in GSCs following siFASTKD2 or siCONT treatment. Representative pseudo-colored images of the ATeam ratio are shown and quantified using a bar graph. (n = 3).

h, ATP levels were measured in TMs of GSCs following FASTKD2 knockdown. (n = 3).

Representative of two independent experiments in b-c. Data are presented from more than three independent experiments in d-h. Data are presented as mean ± SD. Student's t-test with p values for g, One-way ANOVA followed by multiple comparisons with adjusted p values for d-f and h.

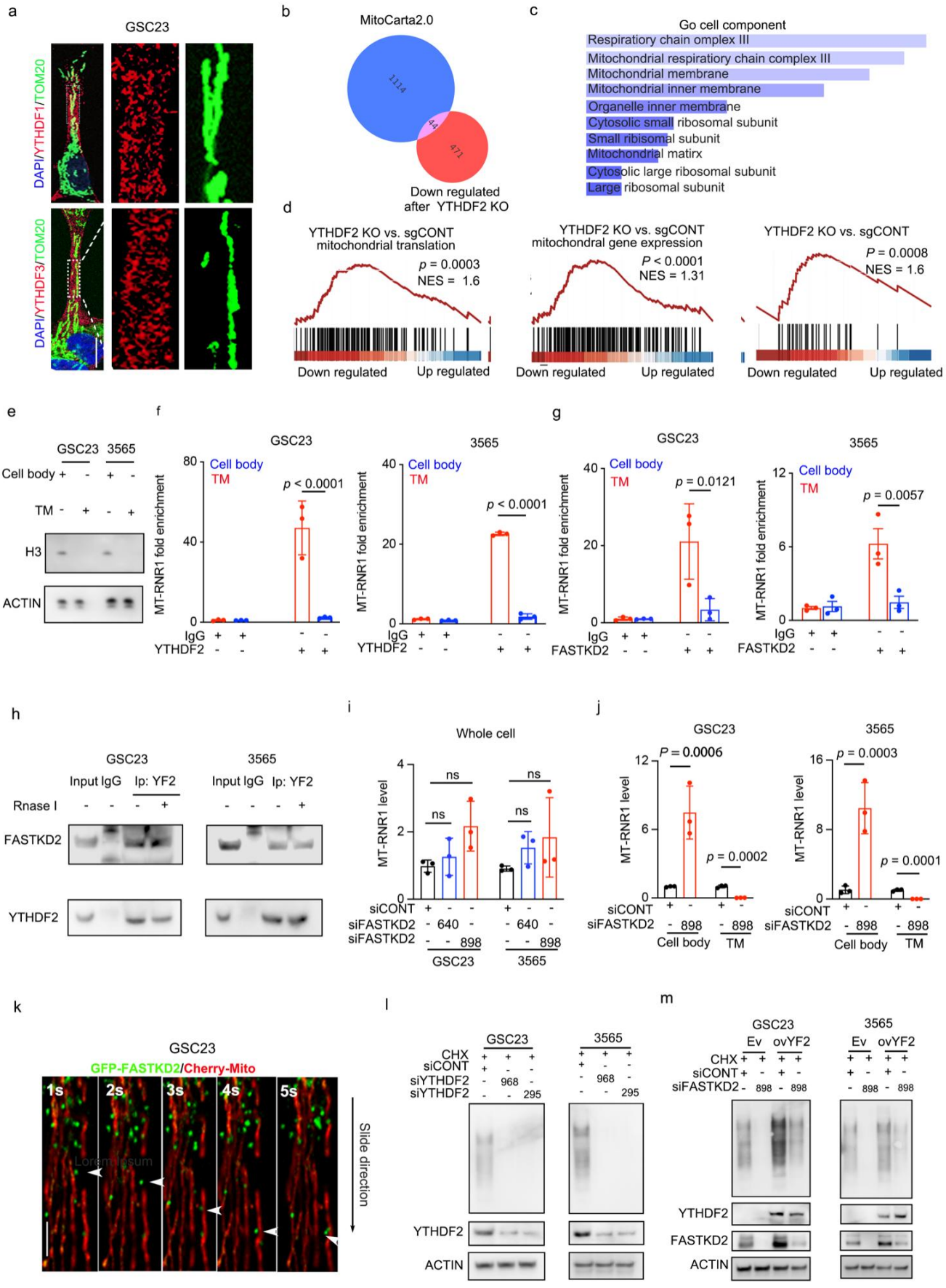
a
GSC23
DAPI/YTHDF1/TOM20
DAPI/YTHDF3/TOM20
b
MitoCarta2.0
1114
44
471
Down regulated
after YTHDF2 KO
c
Go cell component
Respiratory chain omplex III
Mitochondrial respiratory chain complex III
Mitochondrial membrane
Mitochondrial inner membrane
Organelle inner membrane
Cytosolic small ribosomal subunit
Small ribisomal subunit
Mitochondrial matirx
Cytosolic large ribosomal subunit
Large ribosomal subunit
d
YTHDF2 KO vs. sgCONT
mitochondrial translation
p = 0.0003
NES = 1.6
Down regulated
Up regulated
YTHDF2 KO vs. sgCONT
mitochondral gene expression
P < 0.0001
NES = 1.31
Down regulated
Up regulated
YTHDF2 KO vs. sgCONT
P = 0.0008
NES = 1.6
Down regulated
Up regulated
e
GSC23
3565
Cell body
TM
H3
ACTIN
f
GSC23
3565
Cell body
TM
p < 0.0001
MT-RNR1 fold enrichment
IgG
YTHDF2
g
GSC23
3565
Cell body
TM
p = 0.0121
p = 0.0057
MT-RNR1 fold enrichment
IgG
FASTKD2
h
GSC23
3565
Input IgG
Ip: YF2
Rnase I
FASTKD2
YTHDF2
i
Whole cell
MT-RNR1 level
ns
siCONT
siFASTKD2
640
898
GSC23
3565
j
GSC23
3565
P = 0.0006
p = 0.0002
p = 0.0003
p = 0.0001
MT-RNR1 level
siCONT
siFASTKD2
898
Cell body
TM
k
GSC23
GFP-FASTKD2/Cherry-Mito
1s
2s
3s
4s
5s
Slide direction
l
GSC23
3565
CHX
siCONT
siYTHDF2
siYTHDF2
968
295
YTHDF2
ACTIN
m
GSC23
3565
Ev
ovYF2
CHX
siCONT
siFASTKD2
898
YTHDF2
FASTKD2
ACTIN

Extended Data Figure 5. FASTKD2 maintenance of mitochondrial function requires YTHDF2 to stabilize MT-RNR1.

a, Representative imaging of the distribution of YTHDF1 (magenta), YTHDF3 (magenta), and TOM20 (green) in GSC23 TM. Scale bar: 20 μm.

b, Venn diagram illustrating overlapping genes between downregulated genes in YTHDF2 KO and mitochondria-related genes derived from MitoCarta2.0.

c, Functional analysis network of mitochondrial-related genes downregulated in response to YTHDF2 knockout.

d, Gene set enrichment analysis (GSEA) plot indicating enrichment of mitochondrial translation, mitochondrial ribosome, and mitochondrial gene expression pathways in sgCONT as compared to sgYTHDF2 in GSCs.

e, Western blot analysis of TM and cell body separation.

f, RIP-qPCR indicating the interaction between YTHDF2 and MT-RNR1 in mitochondria isolated from the cell body and TM in GSCs. (n = 3).

g, RIP-qPCR indicating the interaction between FASTKD2 and MT-RNR1 in mitochondria isolated from the cell body and TM in GSCs. (n = 3).

h, IP analysis of the interaction between YTHDF2 and FASTKD2 in the presence of Rnase I treatment.

i, Quantification of MT-RNR1 levels in whole cells in the presence or absence of FASTKD2 knockdown. (n = 3).

j, Quantification of MT-RNR1 levels in the cell body and TM in the presence or absence of FASTKD2 knockdown. (n = 3).

k, Time tracking of FASTKD2 along the mitochondrial network in GSC23. Green represents GFP-FASTKD2 and red represents Cherry-mito. Scale bar: 20 μm.

l, Western blot analysis of mitochondrial protein synthesis in TMs following YTHDF2 knockdown.

m, Western blot analysis of mitochondrial protein synthesis in TMs following YTHDF2 overexpression in GSCs.

Representative of two independent experiments in e, h l, and m. Data are presented from three independent experiments in f, g, i and j. Data are presented as mean ± SEM. Two-way ANOVA followed by multiple comparisons with adjusted p-values for f, g, i and j.

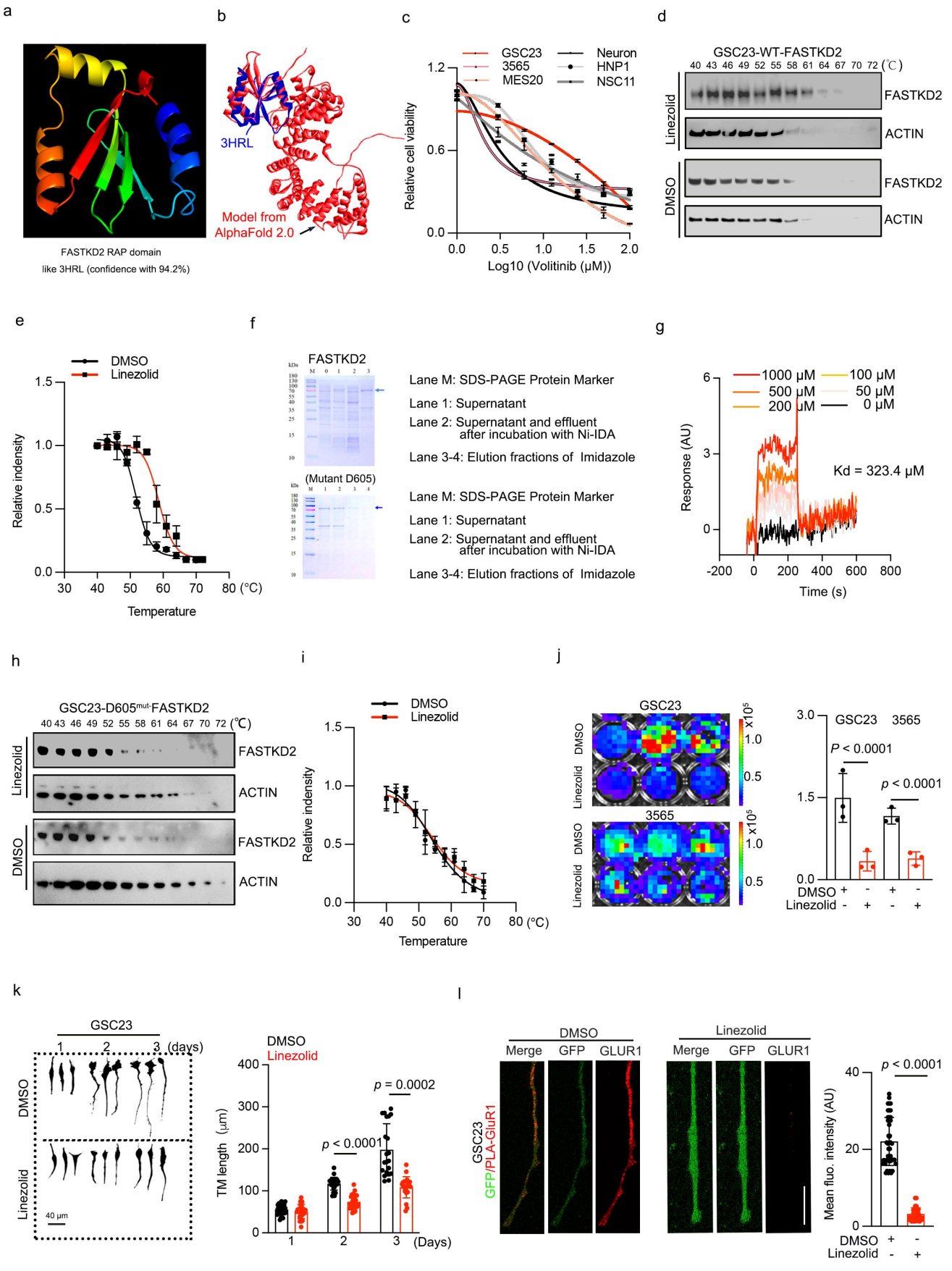
a
b
c
d
FASTKD2 RAP domain
like 3HRL (confidence with 94.2%)
3HRL
Model from
AlphaFold 2.0
GSC23
3565
MES20
Neuron
HNP1
NSC11
Relative cell viability
Log10 (Volitinib (μM))
GSC23-WT-FASTKD2
40 43 46 49 52 55 58 61 64 67 70 72 (℃)
Linezolid
DMSO
FASTKD2
ACTIN
e
f
g
DMSO
Linezolid
Relative indensity
Temperature
FASTKD2
(Mutant D605)
Lane M: SDS-PAGE Protein Marker
Lane 1: Supernatant
Lane 2: Supernatant and effluent
after incubation with Ni-IDA
Lane 3-4: Elution fractions of Imidazole
Lane M: SDS-PAGE Protein Marker
Lane 1: Supernatant
Lane 2: Supernatant and effluent
after incubation with Ni-IDA
Lane 3-4: Elution fractions of Imidazole
1000 μM
500 μM
200 μM
100 μM
50 μM
0 μM
Kd = 323.4 μM
Response (AU)
Time (s)
h
i
j
GSC23-D605mut-FASTKD2
40 43 46 49 52 55 58 61 64 67 70 72 (℃)
Linezolid
DMSO
FASTKD2
ACTIN
Relative indensity
Temperature
GSC23
3565
x10^5
P < 0.0001
p < 0.0001
DMSO
Linezolid
k
l
GSC23
1 2 3 (days)
DMSO
Linezolid
40 μm
TM length (μm)
p = 0.0002
p < 0.0001
(Days)
Merge
GFP
GLUR1
GSC23
GFP/PLA-GluR1
Mean fluo. intensity (AU)
p < 0.0001

Extended Data Figure 6. Pharmacological targeting FASTKD2 suppresses neuronal-glioma interactions and GSC proliferation

a, Structural modeling of the human FASTKD2 protein compared to known PD-(D/E)-XK nucleases. Models and structures are shown as a schematic colored by secondary structure elements.

b, Aligned result between 3HRL and the predicted structure (FASTKD2) from AlphaFold2 using the Discovery Studio software.

c, Cell viability was evaluated in various glioma cell lines (GSC23, MES20, 3565), neural stem cell lines (NSC11, HNP1), and neuron cells upon treatment with increasing concentrations of Volitinib.

d, Cell thermal migration assay showing change in the stability of FASTKD2 in GSC23 when treated with linezolid at different temperatures.

e, Cell thermal migration assay plot to evaluate the binding effect between linezolid and FASTKD2 under different temperatures.

f, Expression, purification, and identification of FASTKD2 (top) and FASTKD2 mutant protein (bottom). The arrow indicates the target protein.

g, Surface plasmon resonance assay was performed to detect the binding affinity between mutant FASTKD2 and linezolid.

h, Cell thermal migration assay showing a change in the stability of mutant FASTKD2 in GSC23 when treated with linezolid at different temperatures.

i, Quantification of the binding effect between linezolid and FASTKD2 under different temperatures.

j, GSC23 was transfected with a luciferase reporter to monitor ATP concentration after Linezolid (100 μM) treatment for 72 hours. (n = 3).

k, Left: TM length was measured following treatment with linezolid (100 μM) or DMSO control for the indicated time. Right: Quantification of the TM length by NeuronJ. Data represent mean ± SEM (n = 20 - 30). Scale bar: 40 μm.

l, Left: Representative imaging of the distribution of nascent GluR1 in TM with or without Linezolid (100 μM) treatment. Right: Mean fluorescence intensity quantification of nascent GluR1 in GSC23 TM. (n = 15).

Representative of two independent experiments in d and h. Data are presented from three independent experiments in

l and k. Data are presented as mean ±SEM for c, e and i. Student's t-test with p-values for l. Two-way ANOVA followed by multiple comparisons with adjusted p-values for j and k.

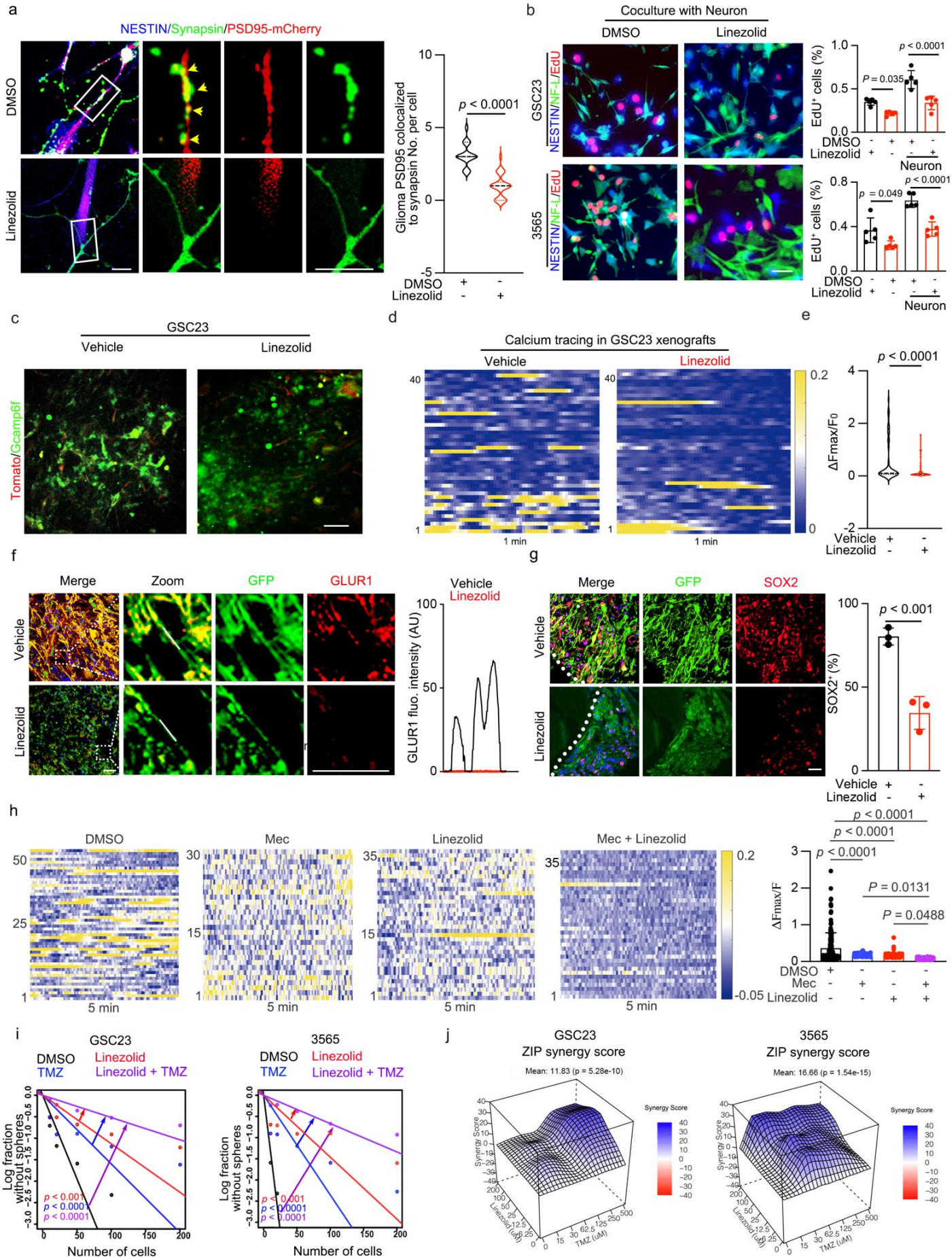
a
NESTIN/Synapsin/PSD95-mCherry
DMSO
Linezolid
Glioma PSD95 colocalized to synapsin No. per cell
p < 0.0001
DMSO
Linezolid
b
Coculture with Neuron
DMSO
Linezolid
GSC23
NESTIN/NF-L/EdU
3565
NESTIN/NF-L/EdU
EdU+ cells (%)
P = 0.035
p < 0.0001
p = 0.049
p < 0.0001
Neuron
c
GSC23
Vehicle
Linezolid
Tomato/Gcamp6f
d
Calcium tracing in GSC23 xenografts
Vehicle
Linezolid
1 min
e
p < 0.0001
ΔFmax/F0
f
Merge
Zoom
GFP
GLUR1
Vehicle
Linezolid
GLUR1 fluo. intensity (AU)
g
Merge
GFP
SOX2
SOX2+ (%)
p < 0.001
h
DMSO
Mec
Linezolid
Mec + Linezolid
5 min
ΔFmax/F
p < 0.0001
p < 0.0001
p < 0.0001
P = 0.0131
P = 0.0488
i
GSC23
3565
DMSO
TMZ
Linezolid
Linezolid + TMZ
Log fraction without spheres
Number of cells
p < 0.001
p < 0.0001
p < 0.0001
j
GSC23
ZIP synergy score
Mean: 11.83 (p = 5.28e-10)
3565
ZIP synergy score
Mean: 16.66 (p = 1.54e-15)
Synergy Score
Linezolid (uM)
TMZ (uM)

Extended Data Fig. 7, Dual inhibition of neuron–glioma connectivity causes synergistic decrease in glioblastoma growth.

a, Left: Representative images of neuron co-culture with glioma cells with and without linezolid pretreatment for 24 hours. NESTIN (glioma, blue), SYNAPSIN (presynaptic puncta, green) and PSD95 (glioma postsynaptic puncta, red) are labeled. Scale bar: 5μm. Right: Post-synaptic glioma-derived PSD95 puncta colocalized with neuronal pre-synaptic synapsin were quantified. (n = 50).

b, Representative immunofluorescence images (left) and proliferation index quantification (right; EdU+ cells/Nestin+ cells) of glioma cells cultured alone or with neurons in the presence or absence of linezolid treatment for 72 hours. (n=5 coverslips per group). Scale bar: 50μm.

c, Representative calcium imaging (120 second time course) of hippocampal slice (n = 3 mice) xenografted with GCaMP6f-expressing glioma with and without linezolid treatment. Scale bar: 50 μm.

d, Heatmap of single-cell Ca^{2+} signals over a 1-min time course in vivo under linezolid treatment.

e, Quantification of the maximal Ca^{2+} response ($\Delta Fmax/F_0$) in GSC23 cells under the linezolidtreatment.

f, Representative immunofluorescence images depicting the downregulated expression of GLUR1(Red) following linezolid treatment in vivo. Scale bar: 40 μm. Right: Quantification the intensity of GlUR1 tumor cells following linezolid treatment.

g, Representative immunofluorescence images depicting the downregulated expression of SOX2 (red) following linezolid treatment in vivo. Scale bar: 40 μm. Right: Quantification of SOX2+ tumor cells following linezolid treatment.

h, Representative heatmaps of Ca^{2+} dynamics in individual cells over a 5-min time course after treatment with linezolid, Mec, or their combination.

Right: Quantification of the maximal Ca^{2+} response ($\Delta Fmax/F_0$) in GSC23 cells under the different treatment conditions.

i, In vitro extreme limiting dilution analysis of GSC tumor sphere formation treated with vehicle control, linezolid (100 μM), temozolomide (500 μM), or

the combination of linezolid and temozolomide. n=3 independent biological cell cultures.

j, 3D synergy landscape plots evaluating the synergistic interaction between linezolid and temozolomide (TMZ). The z-axis represents the synergy score, indicating the degree of synergistic activity. The ZIP model was used to evaluate the mean synergy score.

Representative of two independent experiments in a and b. Data are presented from three independent experiments in c and d. Data are presented as mean ± SD for b, g, h. Student's t-test with p-values for a, e and g. Two-way ANOVA followed by multiple comparisons with adjusted p-values for b and h. ELDA analysis for i.